The Nature of the Oxygen Vacancy in Amorphous Oxide Semiconductors: Shallow Versus Deep

Hochul Song, Gijae Kang, Youngho Kang, and Seungwu Han**

Using first-principles calculation, we investigate the nature of oxygen vacancy (V_O), namely shallow versus deep, in the amorphous oxide semiconductor $InGaZnO_4$ (*a*-IGZO), which has not been fully clarified despite its technological importance. Oxygen-deficient amorphous models are generated through the hybrid functional molecular dynamics (MD) simulations that allow for finding stable V_O configurations while minimizing computational approximations. From eight independent models, we consistently find that V_O serves as the shallow donor, increasing the Fermi level above the conduction band minimum. For comparison purpose, we also generate deep V_O models by charging the system during MD simulations. It is found that deep V_O is higher in the formation energy than shallow V_O, confirming that shallow V_O is the preferred type of oxygen vacancies in *a*-IGZO.

1. Introduction

Owing to the high electron mobility in spite of disordered structures, amorphous oxide semiconductors (AOSs), in particular amorphous $InGaZnO_4$ (*a*-IGZO), have become the channel material in thin-film transistors for high-end commercial displays such as organic-light-emitting-diode (OLED) TV and high-resolution, large-area liquid crystal display (LCD).[1–3] However, various types of device instability are posing hurdles against development of AOSs with higher mobilities.[4,5] In particular, the instability under negative-bias-illumination-stress (NBIS) is known to be most serious.[6,7] Among the suggested mechanisms of the NBIS instability, the oxygen vacancy (V_O) has been receiving intensive attention because AOS films are oxygen deficient.[8–12]

The role of V_O in the device instability critically depends on its nature, specifically, whether defect levels associated with V_O is shallow or deep. For instance, according to a widely cited mechanism,[13] V_O is a deep donor and becomes ionized under visible light. The ionized V_O^{2+} defect then migrates towards the interface with gate dielectrics under the negative bias and becomes hole-trapping sites, sustaining the threshold-voltage shift. On the other hand, if V_O belongs to the shallow donor, it would increase the electrical conductivity but may not be directly involved in NBIS instability.

Because of experimental difficulty in isolating the property of point defects, the density functional theory (DFT) calculations have been useful in investigating V_O in *a*-IGZO.[12–19] However, the conclusion on the nature of V_O is sharply divided; while V_O was found to be dominantly deep in Refs. [13,14,19], shallow property was also claimed in Refs. [12,16,17]. (Refs. [15,18] are inconclusive.) There are two key reasons underlying this controversy. First, the band gap from the conventional DFT is severely underestimated in post-transition metal oxides; the experimental band gap is ≈3.0 eV[12,20] but the local-density approximation (LDA) or generalized-gradient approximation (GGA) yield only 0.5–0.9 eV.[14,15] By applying the on-site Coulomb repulsion (so called $+U$ method), the band gap increases to 1.4–1.8 eV,[14] still far below the experimental gap. Such band-gap underestimation obscures the boundary between the deep and shallow defects, which largely depends on the energy position of defect levels within the band gap, and leads to different conclusions depending on the computational parameters. We also note that the small band gap may unduly favor shallow-type donors by discounting the energy cost for generating defect levels close to the conduction band. Indeed, hybrid functional calculations producing a large band-gap (>3 eV) favored deep states compared to (semi)local functionals.[14,19]

Second, most of the extant theoretical works modeled V_O by removing one oxygen atom from the stoichiometric *a*-IGZO structure that was constructed through melt-quench molecular dynamics (MD) simulations.[12–16] Various defect sites were then sampled and their formation energies were compared. However, due to the inherent meta-stability of amorphous structures, the energetic comparison is not reliable, causing different conclusions among literature. Furthermore, such a way of V_O modeling is at odds with the nature of amorphous structures that the lattice site is ill-defined. That is to say, it is conceivable in amorphous structures that V_O is structurally diffused over a large area, rather than centralized around a localized space. To take this possibility into account, it is necessary to include the oxygen deficiency during generating amorphous models, for instance, melt-quench simulations. A few works tried such

H. Song, G. Kang, Dr. S. Han
Department of Materials Science and Engineering and Research Institute of Advanced Materials
Seoul National University
Seoul 08826, Korea
E-mail: hansw@snu.ac.kr

Dr. Y. Kang
Materials Data Center
Korea Institute of Materials Science
Changwon 51508, Korea
E-mail: thehoya84@gmail.com

DOI: 10.1002/pssb.201800486

approaches in modeling the oxygen-deficient *a*-IGZO,[12,17,18] but the semilocal functional used in the calculation underestimates the band gap, which can bias the result, as explained above.

The foregoing discussion concludes that every calculation in the literature so far suffers from its own computational limitation, which renders the discovered nature of V_O to be disputable. In this work, we explore the nature of V_O in *a*-IGZO, addressing the above drawbacks in the previous calculations, that is, band gap underestimation and post-removal scheme for generating V_O. To this end, we consistently adopt the computationally costive but accurate hybrid functional method throughout the whole melt-quench MD simulations[21] and incorporate the oxygen vacancy from onset of simulations. This approach allows us to identify stable V_O configurations without any bias or constraints, while maintaining the correct band gap. We generate eight oxygen-deficient *a*-IGZO models (*a*-$IGZO_{4-x}$). Without an exception, we find that the Fermi level lies above the conduction band minimum, making it clear that V_O is the shallow donor in *a*-$IGZO_{4-x}$

2. Computational Setup

Throughout this work, the first-principles MD simulations are conducted using the Vienna Ab inito Simulation Package (VASP)[22] version 5.4.1 with the projector-augmented wave (PAW) pseudopotential.[23] The pseudopotential contains the valence electrons of $5s^25p^1$ for In, $4s^24p^1$ for Ga, $3d^{10}4s^2$ for Zn, and $2s^22p^4$ for O. Amorphous structures for both stoichiometric *a*-IGZO and oxygen-deficient *a*-$IGZO_{4-x}$ are generated using the conventional melt-quench process.[24] The *a*-IGZO model contains sixteen $InGaZnO_4$ units (112 atoms in total) and an oxygen atom is removed in *a*-$IGZO_{4-x}$ (111 atoms). First, we put constituent atoms randomly into a cubic box with the length of 11.1 Å, which corresponds to the density of *a*-IGZO in experiment.[20] The initial atomic positions are randomized by premelting at 5000 K for 2 ps, followed by melting at 2500 K for 10 ps, and they are quenched to 500 K with a constant cooling rate of $-500\,K\,ps^{-1}$. The final structure is fully relaxed until the magnitude of atomic forces are reduced to within $0.05\,eV\,Å^{-1}$. The energy cutoff for the plane-wave basis is chosen to be 250 and 500 eV for MD and relaxation steps, respectively. (During MD, a soft PAW pseudopotential was used for O atoms, which reduced the energy cutoff). To reflect the disorder in amorphous structures in a statistical way, we obtain eight models of *a*-$IGZO_{4-x}$. For the comparison purpose, we also generate two stoichiometric *a*-IGZO (*a*-$IGZO_4$) models following the same melt-quench procedure.

We employ the hybrid functional of the Heyd-Scuseria-Ernzerhof (HSE) type[25,26] through the whole calculations. The fraction of the exact exchange energy is set to 0.32, tuning to the experimental band gap for crystalline $InGaZnO_4$ (3.5 eV).[27] This produces 2.9 eV for the band gap of the stoichiometric *a*-IGZO, which is in good agreement with experimental values.[12,20] The smaller band gap of *a*-IGZO than for the crystalline phase is attributed to the downshift of the conduction band, as discussed in the previous work.[28] For the Brillouin-zone integration, only the Γ point is sampled, which allows us to avoid the band-filling problem.[29] Since the conduction band is highly dispersive and its minimum (CBM) appears at Γ, the band-filling problem becomes serious in calculations of shallow defects using a finite supercell. (Note that we are aiming at identifying the defect property in the dilute limit, that is, low oxygen deficiency).

3. Results and Discussion

We first discuss structural properties of *a*-$IGZO_{4-x}$. **Figure 1** shows the pair distribution functions $[g(r)]$ for metal-oxygen (M-O) and metal-metal (M-M) pairs that are averaged over ions within the generated models. For comparison, $g(r)$ for *a*-IGZO is also shown. It is seen that the first peak is pronounced, implying that the short-range order is well maintained like the crystalline phase. In Figure 1, $g(r)$'s for *a*-$IGZO_{4-x}$ and *a*-$IGZO_4$ are almost identical, indicating that the oxygen deficiency does not cause any substantial change in the amorphous structure, for instance additional M-M bonds. This is also confirmed by the M-O bond lengths and coordination numbers in **Table 1**, which shows analogous results between *a*-$IGZO_4$ and *a*-$IGZO_{4-x}$. They are also in good agreements with previous theoretical results using the semilocal functional[28] and EXAFS analysis.[30]

Even though the present work consistently employs the hybrid functional, we find that the small supercell still prohibits clear-cut distinction of the defect type. In particular, the electronic coupling between highly dispersive conduction state and localized state can make it difficult to assess the defect type purely based on the energy of defect levels. In order to draw a definite conclusion, we determine the nature of V_O by examining the band dispersion and spatial distribution of the highest occupied state, in addition to its energy level within the band gap. (Strictly speaking, the Bloch vector is not well defined in the amorphous structure. However, pseudo band-structures of the given supercell are useful to examine the delocalization).[31] The degree of delocalization can be quantified by the inverse participation ratio (IPR) as follows[32]:

$$\mathrm{IPR} = \frac{\sum_i^N \omega_i^2}{\left(\sum_i^N \omega_i\right)^2} \tag{1}$$

where N is the total number of atoms in the supercell and w_i is the partial weight of the given state on the i-th atom. If the state is evenly distributed over entire atoms, IPR becomes $1/N$, while it

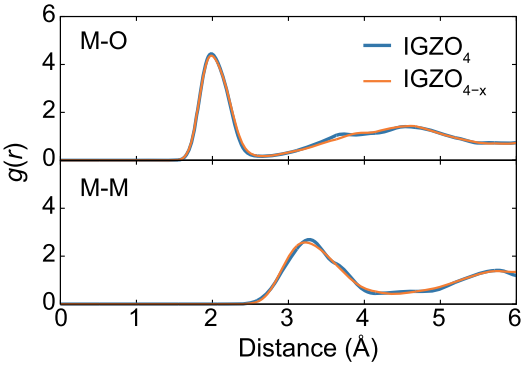

Figure 1. Ion-averaged pair distribution functions for metal–oxygen (M–O) and metal–metal (M–M) pairs in *a*-$IGZO_{4-x}$ and *a*-$IGZO_4$.

Table 1. Averaged values of the bond length (r) between metal and oxygen ions and coordination numbers (N_c) around metal ions in a-$IGZO_{4-x}$. The values in the parenthesis are for a-$IGZO_4$.

	This work		Cal. (ref. [28])		Exp. (ref. [30])	
	r [Å]	N_c	r [Å]	N_c	r [Å]	N_c
In-O	2.17 (2.17)	5.79 (5.95)	2.19	5.58	2.30	5.80
Ga-O	1.90 (1.91)	4.89 (4.85)	1.93	4.71	1.93	4.90
Zn-O	1.99 (2.00)	4.51 (4.39)	1.98	4.28	1.99	4.50

approaches one when it is localized over a few atomic sites. Based on the definition of IPR in Equation (1), if V_O develops a dispersive band with low IPR values, it is regarded as shallow, while the flat band with high IPR indicates the deep character.

The band structure of a-$IGZO_4$ is plotted in **Figure 2**a. The valence band consists of mainly O-p states, while metal s states comprises the conduction band. The bands near the valence band maximum (VBM) exhibit flat dispersions, implying those states are spatially localized over a few atomic sites. This is consistent with the high IPR values in the right figure. This arises from inefficient hybridization between O-p states in disordered structures due to the directionality and the small size of O-p orbitals. In contrast to the valence band, the lowest conduction band shows a significant dispersion because the overlap between the large and spherical metal s states is insensitive to the directional disorder. In particular, the well-ordered first coordination shell results in a quasi-linear conduction band, which is generally discovered in oxides containing In, Ga, Zn, and Sn.[31] The low IPR values (see the dashed ellipsoid) is much lower than for those around VBM, supporting the delocalized nature.

The band structure for an a-$IGZO_{4-x}$ model is shown in Figure 2b. It is seen that the band structure is similar to that of a-$IGZO_4$ in Figure 2a, and no pronounced defect level is identified within the band gap. The lack of an oxygen atom results in two electrons occupying the conduction band, raising the Fermi level above the CBM. The IPR values for the highest occupied band (see the dashed ellipsoid) are similar to the CBM in Figure 2a. This implies that the oxygen vacancy act as shallow donors. For every eight model of a-$IGZO_{4-x}$, we consistently obtain the electronic structure similar to Figure 2b, confirming the shallow nature of V_O unequivocally.

For the comparison purpose, we artificially generate deep V_O by charging the supercell with two extra electrons during the melt-quench simulation. The extra electrons facilitate the formation of a deep level, which helps reduce the band energy. At the end of the melt-quench simulation, we remove the additional electrons and carry out the structural relaxation. Out of eight trials, we obtain five a-$IGZO_{4-x}$ models that develop a deep V_O state. **Figure 3**a exhibits the band structure for one of the deep V_O models. The deep defect level is clearly seen within the band gap (see the arrow). The IPR value in the dashed ellipsoid indicates strong localization. This can be directly confirmed by the charge density distribution of this state in Figure 3b. It is found that the state is well confined between two In atoms that are separated by 2.9 Å. For other cases, the deep level always develops at weak bonding between metal atoms involving at least one In atom. Consistently, in previous calculations that analyzed the bonding environments around V_O,[14,19] it was revealed that the defect formation energy is lower when V_O is surrounded by In atoms. Among the five models, defect levels are scattered over 1.7–2.1 eV from CBM.

To compare the stability of shallow and deep V_O, we calculate the defect formation energy (E_{for}) according to the following formula:

$$E_{for} = E(a\text{-}IGZO_{4-x}) - \bar{E}(a\text{-}IGZO_4) + \mu_O \quad (2)$$

where $E(a\text{-}IGZO_{4-x})$ is the total energy of an a-$IGZO_{4-x}$ model and $\bar{E}(a\text{-}IGZO_4)$ is the ensemble average of the total energy over two stoichiometric models. More sampling of stoichiometric structures would change $(\bar{E}(a\text{-}IGZO_4))$ to some extent, but the main conclusion would not be affected much because it is a common reference. In Equation (2), μ_O is the oxygen chemical potential, which is set to the half of the total energy of an O_2 molecule. **Figure 4**a shows the calculated E_{for} for deep and shallow V_O models (five and eight, respectively). Because of the structural fluctuation in the amorphous models, E_{for} varies substantially among the samples. The average energy of the shallow V_O models are more stable than the deep V_O models by 1.22 eV, which confirms that the shallow V_O is indeed the preferred type of oxygen vacancies in a-IGZO. The relative stability can also be confirmed by the simulated annealing; for deep V_O models, we anneal the system at 600 K and find that every model converts to shallow one within 5 ps. Figure 4b shows the

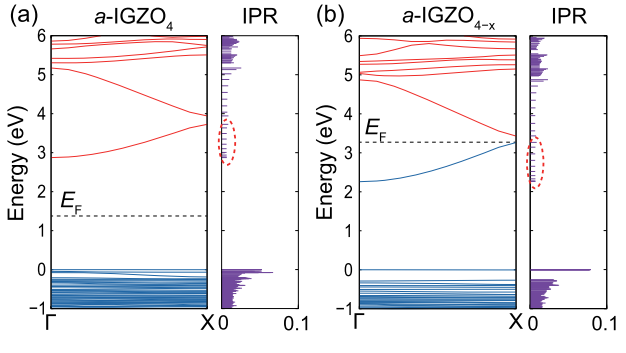

Figure 2. Calculated band structures and inverse participation ratio (IPR) of electronic states for (a) a-$IGZO_4$ and (b) a-$IGZO_{4-x}$. The Fermi level (E_F) is shown as dashed lines. The IPR values of delocalized conduction states are marked in dashed ellipsoid.

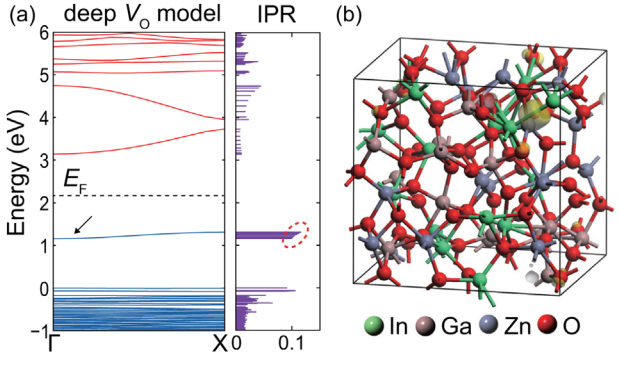

Figure 3. a) Calculated band structure and IPR for a deep V_O model. The arrow indicates the deep state associated with V_O and its IPR values are marked in dashed ellipsoid. Isosurface in (b) is the distribution of the charge density of the deep level.

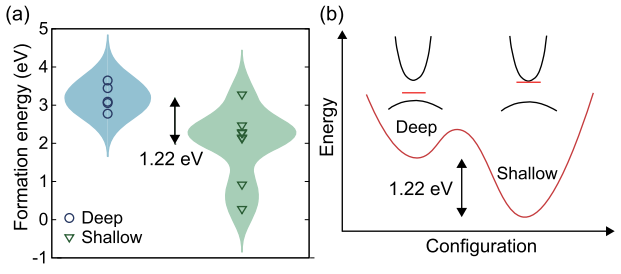

Figure 4. a) Formation energy of deep and shallow oxygen vacancies. The shaded area represents the distribution of oxygen vacancy formation energy obtained by applying Gaussian broadening with a standard deviation of 0.4 eV. b) Schematic energy-configuration diagram for oxygen vacancies in *a*-IGZO.

schematic energy-configuration diagram for V_O in *a*-IGZO as inferred from the present computation.

The majority of the V_O in *a*-IGZO films is expected to serve as the shallow donor contributing to the *n*-type conductivity. This is consistent with experimental results in which *a*-IGZO films grown under oxygen-poor conditions exhibit higher carrier concentrations.[1] Although metastable, deep V_O could also be present in films, but should be low in concentration. Accordingly, V_O may not be a main source causing the device instability under NBIS, and other alternative mechanisms related to hydrogen impurities[6] or peroxide formation[33,34] are therefore worth close attention.

4. Conclusion

In conclusion, we investigated the nature of V_O in *a*-IGZO using first-principles calculations. To circumvent the two modeling issues associated with the band gap and vacancy configuration, the hybrid density functional MD simulations were employed to generate oxygen deficient amorphous models. Our analysis on the electronic structure and energetics of V_O models showed that the majority of oxygen vacancies acts as shallow donors in *a*-IGZO. By establishing the nature of oxygen vacancies, this work may help to resolve the stability problems of AOS thin film transistors.

Acknowledgements

Hochul Song and Gijae Kang contributed equally to this work. This work was supported by the Technology Innovation Program (or Industrial Strategic Technology Development Program [10052925, Atomistic process and device modeling of sub-10 nm scale transistors]) funded by the Ministry of Trade, Industry & Energy (MOTIE, Korea) and Creative Materials Discovery Program through the National Research Foundation of Korea (NRF) funded by Ministry of Science and ICT (2017M3D1A1040689). The computations were carried out at the KISTI Supercomputing Center (KSC-2018-C3-0022).

Keywords

computational physics, density functional theory, hybrid functional, $InGaZnO_4$, oxygen vacancy

Received: September 17, 2018
Revised: October 16, 2018
Published online: December 3, 2018

[1] H. Kumomi, K. Nomura, T. Kamiya, H. Hosono, *Thin Solid Films* **2008**, *516*, 1516.
[2] T. Kamiya, H. Hosono, *NPG Asia Mater.* **2010**, *2*, 15.
[3] J. Sheng, H. J. Jeong, K. L. Han, T. Hong, J. S. Park, *J. Inf. Disp.* **2017**, *18*, 159.
[4] J. K. Jeong, *Semicond. Sci. Technol.* **2011**, *26*, 034008.
[5] N. On, Y. Kang, A. Song, B. Du Ahn, H. D. Kim, J. H. Lim, K. B. Chung, S. Han, J. K. Jeong, *IEEE Trans. Electron Devices* **2017**, *64*, 4965.
[6] Y. Kang, B. D. Ahn, J. H. Song, Y. G. Mo, H. H. Nahm, S. Han, J. K. Jeong, *Adv. Electron. Mater.* **2015**, *1*, 1400006.
[7] J. Bang, S. Matsuishi, H. Hosono, *Appl. Phys. Lett.* **2017**, *110*, 232105.
[8] H. Song, Y. Kang, H. H. Nahm, S. Han, *Phys. Status Solidi B* **2015**, *252*, 1872.
[9] M. D. H. Chowdhury, P. Migliorato, J. Jang, *Appl. Phys. Lett.* **2010**, *97*, 173506.
[10] S. Yang, K. H. Ji, U. K. Kim, C. S. Hwang, S. H. Ko Park, C. S. Hwang, J. Jang, J. K. Jeong, *Appl. Phys. Lett* **2011**, *99*, 102103.
[11] Y. J. Tak, D. H. Yoon, S. Yoon, U. H. Choi, M. M. Sabri, B. D. Ahn, H. J. Kim, *ACS Appl. Mater. Interfaces* **2014**, *6*, 6399.
[12] T. Kamiya, K. Nomura, M. Hirano, H. Hosono, *Phys. Status Solidi C* **2008**, *5*, 3098.
[13] B. Ryu, H. K. Noh, E. A. Choi, K. J. Chang, *Appl. Phys. Lett.* **2010**, *97*, 022108.
[14] H. K. Noh, K. J. Chang, B. Ryu, W. J. Lee, *Phys. Rev. B* **2011**, *84*, 115205.
[15] T. Kamiya, K. Nomura, H. Hosono, *Phys. Status Solidi A* **2009**, *206*, 860.
[16] A. de Jamblinne de Meux, A. Bhoolokam, G. Pourtois, J. Genoe, P. Heremans, *Phys. Status Solidi A* **2017**, *214*, 1600889.
[17] I. J. Kang, C. Park, **2011**, *arXiv preprint arXiv:1108.2086.*
[18] T. Kamiya, K. Nomura, H. Hosono, *Phys. Status Solidi A* **2010**, *207*, 1698.
[19] H. Li, Y. Guo, J. Robertson, *Phys. Rev. Mater.* **2018**, *2*, 074601.
[20] T. Kamiya, K. Nomura, H. Hosono, *J. Disp. Technol.* **2009**, *5*, 468.
[21] K. Y. Kim, D. Y. Cho, B. K. Cheong, D. Kim, H. Horii, S. Han, *J. Appl. Phys.* **2013**, *113*, 134302.
[22] G. Kresse, J. Furthmüller, *Phys. Rev. B* **1996**, *54*, 11169.
[23] G. Kresse, D. Joubert, *Phys. Rev. B* **1999**, *59*, 1758.
[24] Y. Youn, Y. Kang, S. Han, *Comput. Mater. Sci.* **2014**, *95*, 256.
[25] J. Heyd, G. E. Scuseria, M. Ernzerhof, *J. Chem. Phys.* **2003**, *118*, 8207.
[26] J. Heyd, G. E. Scuseria, M. Ernzerhof, *J. Chem. Phys.* **2006**, *124*, 219906.
[27] M. Orita, M. Takeuchi, H. Sakai, H. Tanji, *Jpn. J. Appl. Phys.* **1995**, *34*, L1550.
[28] Y. Kang, H. Song, H. H. Nahm, S. H. Jeon, Y. Cho, S. Han, *APL Mater.* **2014**, *2*, 032108.
[29] W. J. Yin, J. Ma, S. H. Wei, M. M. Al-Jassim, Y. Yan, *Phys. Rev. B* **2012**, *86*, 045211.
[30] D. Y. Cho, J. Song, K. D. Na, C. S. Hwang, J. H. Jeong, J. K. Jeong, Y. G. Mo, *Appl. Phys. Lett.* **2009**, *94*, 112112.
[31] Y. Kang, S. H. Jeon, Y. W. Son, Y. S. Lee, M. Ryu, S. Lee, S. Han, *Phys. Rev. Lett.* **2012**, *108*, 196404.
[32] E. Cho, S. Han, D. Kim, H. Horii, H. S. Nam, *J. Appl. Phys.* **2011**, *109*, 043705.
[33] H. H. Nahm, Y. S. Kim, D. H. Kim, *Phys. Status Solidi B* **2012**, *249*, 1277.
[34] Y. Kang, H. H. Nahm, S. Han, *Sci. Rep.* **2016**, *6*, 35148.